Single-cell adhesion probed in-situ using optical tweezers: A case study with Saccharomyces cerevisiae

Mickaël Castelain, P. G. Rouxhet, F. Pignon, Albert Magnin, Jean-Michel Piau

Single-cell adhesion probed in-situ using optical tweezers: A case study with Saccharomyces cerevisiae

Mickaël Castelain, Paul G. Rouxhet, Frédéric Pignon, Albert Magnin, and Jean-Michel Piau

Citation: J. Appl. Phys. **111**, 114701 (2012); doi: 10.1063/1.4723566
View online: http://dx.doi.org/10.1063/1.4723566
View Table of Contents: http://jap.aip.org/resource/1/JAPIAU/v111/i11
Published by the American Institute of Physics.

Single-cell adhesion probed *in-situ* using optical tweezers: A case study with *Saccharomyces cerevisiae*

Mickaël Castelain,[1,2,a)] Paul G. Rouxhet,[3] Frédéric Pignon,[1] Albert Magnin,[1] and Jean-Michel Piau[1]
[1]*Laboratoire de Rhéologie, Institut National Polytechnique de Grenoble, Université Joseph Fourier Grenoble I, CNRS, UMR 5520, B.P. 53, F-38041 Grenoble Cedex 9, France*
[2]*Department of Physics, Umeå University, SE-90187 Umeå, Sweden*
[3]*Institute of Condensed Matter and Nanosciences—Bio & Soft Matter, Université catholique de Louvain, Croix du Sud 1, Box L7.04.01, B-1348 Louvain-La-Neuve, Belgium*

(Received 18 September 2011; accepted 29 April 2012; published online 1 June 2012)

A facile method of using optical trapping to measure cell adhesion forces is presented and applied to the adhesion of *Saccharomyces cerevisiae* on glass, in contact with solutions of different compositions. Trapping yeast cells with optical tweezers (OT) is not perturbed by cell wall deformation or cell deviation from a spherical shape. The trapping force calibration requires correction not only for the hydrodynamic effect of the neighboring wall but also for spherical aberrations affecting the focal volume and the trap stiffness. Yeast cells trapped for up to 5 h were still able to undergo budding but showed an increase of doubling time. The proportion of adhering cells showed the expected variation according to the solution composition. The detachment force varied in the same way. This observation and the fact that the detachment stress was exerted parallel to the substrate surface point to the role of interactions involving solvated macromolecules. Both the proportion of adhering cells and the removal force showed a distribution which, in our experimental conditions, must be attributed to a heterogeneity of surface properties at the cell level or at the subcellular scale. As compared with magnetic tweezers, atomic force microscopy, and more conventional ways of studying cell adhesion (shear-flow cells), OT present several advantages that are emphasized in this paper. © *2012 American Institute of Physics*.
[http://dx.doi.org/10.1063/1.4723566]

I. INTRODUCTION

Light, under certain conditions, exerts minute forces that provide a way to manipulate and transport micrometer- to nanometer-sized objects within a fluid medium. This concept gives rise to optical tweezers (OT) techniques.[1] OT provide a powerful, sterile, and noninvasive tool for the manipulation of cells, single macromolecules[2] and colloidal particles,[3] and manipulation of small structures inside intact cells with the exclusive use of light.[4] Since the technique can measure forces ranging from sub-picoNewton (pN) up to several hundreds of pN with good precision (<1 pN), it is applicable to interfacial interactions and non-covalent bonds, e.g., receptor-ligand bonds.[5]

Microbial adhesion is controlled by the interplay of various forces. Specific forces are governed by the "key-lock" system and can exhibit a rupture force level in the order of 100 pN. They have been measured by atomic force microscopy[6] (AFM), shear-flow chamber,[7] and optical tweezers.[5] On the other hand, non-specific forces are widely described in the literature, mainly in the frame of the Derjaguin-Landau-Verwey-Overbeek theory (DLVO). However, although this theory as well as the extended-DLVO (Ref. 8) are extensively used for describing biological systems, these approaches have to be considered vigilantly since they rely on simplistic conditions such as rigid, smooth, non porous, and chemically inert surfaces.

Physical, chemical, and biological factors, governing the critical steps of the primary adhesion of microbial communities in aqueous media, have been intensively studied: hydrophobic interactions,[9,10] substrate roughness,[11] physicochemical properties of the suspending medium,[12] surface charge,[13] and macromolecules emanating from the cell surface,[14] with the possible influence of growth conditions and growth phase.[15–17]

The influence of surrounding solution is of particular interest to understand the cell adhesion. Previous works[18–22] have shown the influence of ionic strength (IS) on bioadhesive behavior of yeast cells to glass. Increasing IS leads to reduction of the electrical double-layer thickness.

Due to stochastic fluctuations in gene expression, referred to as genetic noise, a phenotypic heterogeneity remains and cannot be resolved by measuring the average response of a population, for example, in a flow chamber. As compared with shear-flow chamber measurements, which are bulk methods, single-cell measurements with OT are more suitable to trace the distribution of the force needed to remove the cells in a population.

The aim of this paper is to strengthen the methodology and to evaluate the use of OT for determining the ability of

[a)]Author to whom correspondence should be addressed. Electronic mail: mickael.castelain@insa-toulouse.fr. Present address: Laboratoire d'Ingénierie des Systèmes Biologiques et Procédés (LISBP), INSA Toulouse, 135 Avenue de Rangueil, F-31077 Toulouse Cedex 4, France.

living cells to adhere to a substrate and quantifying the shear force that is required to detach the cells. Prompted by probing at the single-cell scale, home-built Fällman-type optical tweezers[23] enables to manipulate micro-sized living or inert objects and to quantify removal/adhesive forces.[5,18] The fully sequenced yeast cell *Saccharomyces cerevisiae* was selected as a model widespread in agroindustry to study biofilm formation[24] and to examine the effect of hydrodynamics on removal during the early stages of adhesion.[11,20–22] Glass was taken as a common hydrophilic substrate. The influence of experimental factors was examined, selecting factors expected to be crucial, namely, the ionic strength and the nature of the counter-ion in the solution (Ca compared to Na).

II. MATERIALS AND METHODS

A. Yeast cells

Dried baker yeast, *S. cerevisiae* has been provided by Lesaffre (Marcq-en-Baroeul, France) and cultured as described previously.[18,19] Cells were harvested by centrifugation, washed twice with a saline solution (NaCl 1.5, 150, 180, 200, 250, or 330 mM ionic strength—IS; $CaCl_2$ 1.5, 50, 80, 100, 150, 200, or 330 mM ionic strength), suspended again and diluted with the desired solution just before starting the experiment (4×10^6 cells/ml). The final *p*H was 5.9. It is considered that OT is a nearly non-invasive technique. To validate this assumption under the present conditions (laser power, objective, and temperature), cells were trapped individually and the growth of each cell was monitored with a CCD video camera. Therefore, a volume of yeast suspension was collected after 19 h of cultivation, i.e., during exponential growth phase. This volume was then inoculated into a new sterile broth medium. Twenty five microliters of this new suspension were mounted on a coverslip under sterile conditions. The temperature of the sample was set at 30 °C.

Electrophoretic mobility of yeast cells was measured using a Malvern Zetasizer 4 instrument (Malvern, UK, electric field 100 V). The electrophoretic mobility was converted into zeta-potential (ζ) using the Helmoltz-Smoluchowski equation.[8] In order to get the zeta-potential as function of the IS, the yeast cells were suspended in the desired saline solution at about 10^7 cells/ml and the *p*H was adjusted with HCl to 5.9. All measurements were carried out at 25.5 ± 0.1 °C. The values are an average of 5–10 experiments. To circumvent sedimentation effect, the measurements did not last more than 2 min each. The sedimentation rate was estimated from Stokes' law to be about 0.072 mm/min (density of yeast cells considered to be 1.07 g/cm^3,[25] equal to the value deduced for bacteria[26]).

B. Glass substrate

The substrate used was an $18 \times 24 \times 0.17$ mm^3 microscope glass coverslip (Marienfeld-Superior, Marienfeld Laboratory glassware, Lauda-Koenigshofen, Germany). The coverslips were carefully cleaned with a sulfochromic mixture ($K_2Cr_2O_7$ (2.7 M)/H_2SO_4(4% v/v), Chimie Plus Laboratoires, Denicé, France) for 1 h, rinsed three times with distilled water, and immediately stored in Milli-Q water at room temperature. A new clean plate was used for each test and dried just before the test. The surface properties were determined in a previous work.[18]

Finely powdered glass particles were prepared manually by wet grinding in a ball mill for 6 h. The powder was stored in Milli-Q water. Prior to zeta-potential measurements (same procedure as yeast), the suspension was washed three times with the degassed desired saline solution, using a 5 min sonication (Bandelin Sonoplus HD2200) between each centrifugation. The final size was 7.1 ± 1.6 μm. The *p*H and temperature were adjusted as described above. The values are an average of 5-10 experiments. Unless stated otherwise, to circumvent sedimentation effect, the measurements did not last more than 2 min each. The sedimentation rate was estimated to be 0.33 mm/min (density of glass assumed to be 1.2 g/cm^3).

C. Optical tweezers

The experimental set-up is capable of trapping micrometer-sized objects with a refractive index different from those of the suspending medium. A single-beam home-built Fällman-type OT (Ref. 23) system used was described previously.[18,27] A sketch is given in Figure 1(a). The 810-nm laser beam is strongly focused by a microscope objective (Olympus UPLANAPO100xOI) with 1.4 numerical aperture and 48% transmission determined at this wavelength, which is slightly different from the value of 58% provided by the manufacturer. The methodology for assessment of the transmission of this objective was described previously.[28] The power inside the sample is deduced from the power measured before the objective P_B (Molectron PowerMax 500 A with PM10 Probe, Molectron, Portland, OR) and the transmission coefficient of the objective T_O, i.e., $P_{obj} = P_B\ T_O$. This computation insures that experiments are performed in reproducible conditions and avoids any important systematic error regarding the relationships between laser power and trap force.

Two procedures can be used to change the trap position with respect to the substrate along the *x*-, *y*-, *z*-axes, either shifting the laser beam with steering motors or moving the sample with a 3D-piezo-stage (Tritor 3D 101SG, Piezosystem Jena GmbH, Jena, Germany, or E-710.3CD, Physik Instrumente, Karlsruhe, Germany). The sample was sealed between slide and coverslip with a 250-μm thick adhesive spacer (Geneframe 25 μl, ABgene, Epsom, UK) and held on the piezostage. A thermal exchanger was designed to hold the sample and adapted to the piezostage. The temperature-controlled chamber sets the temperature inside the sample at 25.5 ± 0.1 °C.

In addition to micromanipulation, OT can also be used as a tool to apply forces to micrometer-sized objects, including cells and bacteria.[29,30] The conversion of laser power into force was performed by holding a non-adhering single cell with the laser in an immobile position and then moving the piezostage back and forth according to a triangular waveform of amplitude *A* and frequency *f* along x axis parallel to the substrate surface. This generated a laminar flow giving constant back-and-forth velocities *U* over one period,

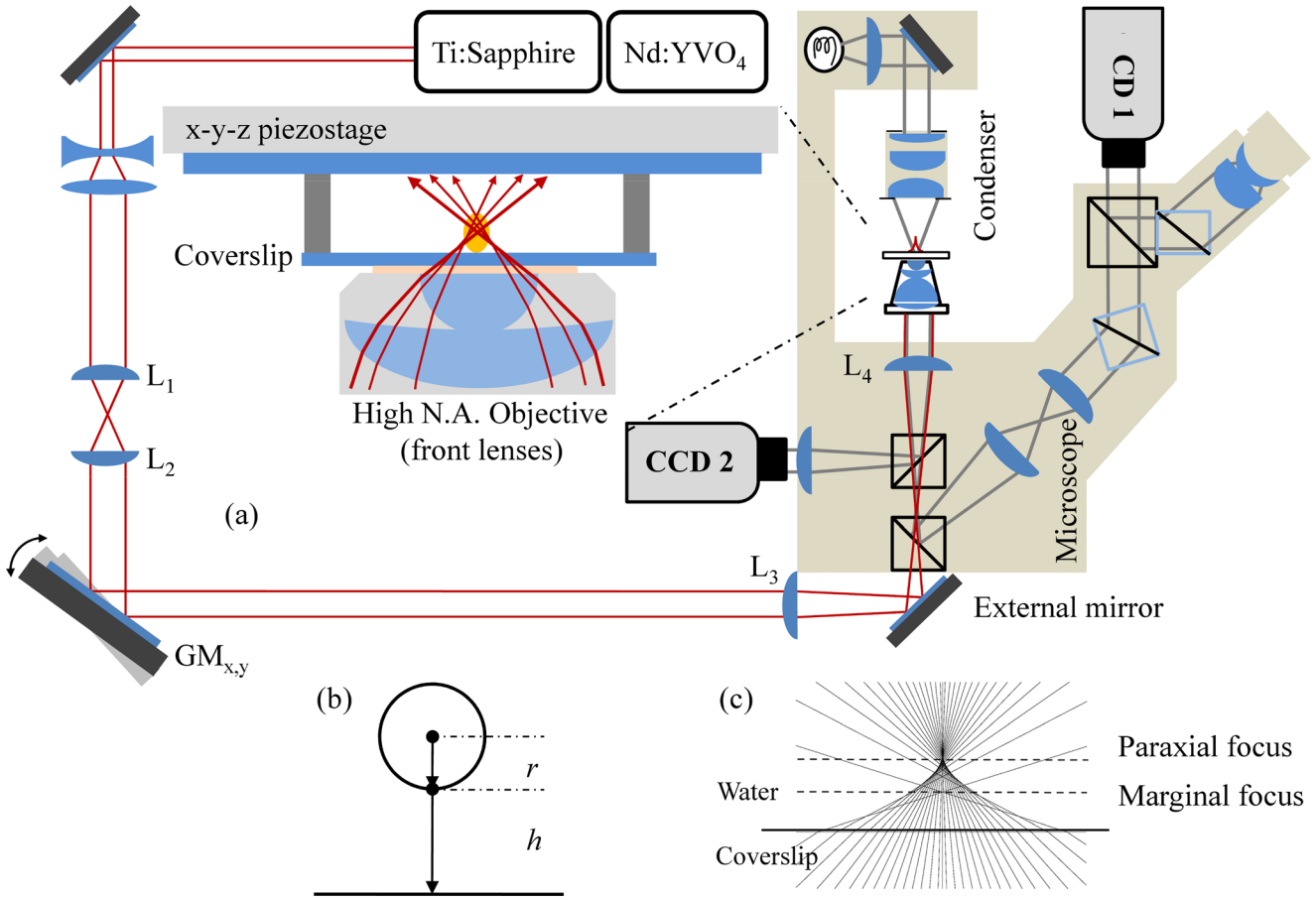

FIG. 1. (a) Simplified schematic layout of the optical tweezers system. (b) Sketch showing the trapped bead (radius r) with respect to the surface at height h. (c) Ray-tracing representation of the refracted trapping beam, showing a shift between the marginal rays and the paraxial rays, which is responsible for an elongated focal volume (spherical aberration).

imposed by the frequency of the oscillation. In this situation, the major cell axis oriented along the flow direction. The frequency was increased until the particle escaped from the trap. When escape occurred, the drag force F_{drag} exerted on the particle was equal to the force F_{trap} exerted by the laser beam.[18,31] According to Stokes law, with a spherical particle and in absence of wall effect,

$$F_{trap} = F_{drag} = 6\pi\eta r U = 12\pi\eta r A f, \qquad (1)$$

where η is the dynamic viscosity of the suspending medium and r the radius of the particle.

The whole setup was controlled via custom-written software programmed in LabVIEW® (National Instruments, Austin, USA) and a 16-bit data acquisition card (NI PCI-6259 M series, National Instruments, Austin, USA). Acquisition of the position of the particle was recorded on a CCD-video camera (CCD-2 in Fig. 1). This information was then used by the automatic software in order to increase the frequency of oscillation until ejection is automatically detected. This procedure lasted 5-10 s. The program also used the dimensions of the particle, the temperature, the viscosity of the suspending medium, the distance to the wall, in order to appropriately post-process the final trap force. Corrections and refinements on the post-processed determination of the force will be discussed below.

D. Application to yeast adhesion

To prepare a sample, 25 μl of yeast suspension (4×10^6 cells/ml) were mounted on a coverslip. Unless stated otherwise, the measurements were performed at 25.5 ± 0.1 °C. The full protocol was described previously.[18] The measurements started after 1 h and were performed sequentially on 30 individual cells, which took 5 to 10 min.

Each cell was examined as follows. The optical trap was placed on the cell and adjusted at 3 μm from the surface (along the z-axis), this distance corresponding to the yeast radius. With a set laser power, an attempt was made to remove the cell from the coverslip by moving the laser beam back and forth with amplitude of approximately 5 μm along the x axis and a frequency of 1 Hz. The laser power at the objective exit was initially set at its lowest level (27 mW) for each yeast cell and then gradually increased up to cell detachment, without going above 120 mW. Cell detachment was easily detected by the fact that the cell was then following the laser oscillation. Moreover, while the adhering cell was oriented with its major axis parallel to the substrate surface, the major axis aligned along the optical axis after detachment. The laser power characteristic of the cell removal was noted. The force needed for cell detachment was deduced from the removal laser power by the calibration mentioned above. Typically, at 120 mW, the loading rate applied on yeast cells during detachment was about 25 pN/s.

III. METHODOLOGICAL ASPECTS

This section presents the methodology used to convert OT measurements into a force required to detach an adhering cell, i.e., the removal force. This involves an evaluation of the corrections needed to account for the influence of the cell shape and of the substrate vicinity. Furthermore, the OT technique is evaluated regarding the possible photodamage on the cells in order to validate the method as non-invasive.

A. Application of Stokes equation

1. Cell wall rigidity

The assumption that a yeast cell behaves as a rigid body, which is implicit in using Stokes law, is acceptable according to Smith *et al.*[32] Indeed, the cell wall of the yeast in the stationary growth phase exhibits a Young's modulus of 107 ± 6 MPa at the single-cell scale, which corresponds to a rather hard material fulfilling Stokes drag requirements. In addition, according to our observations, the particle did not visibly deform during the handling and calibration assays. Consequently, the elasticity of the yeast cells was considered to be negligible with respect to the stresses imposed and was not further considered in the force calibration.

2. Influence of cell shape

Before each force calibration, the dimensions of the trapped cell were determined on the screen, using the NI-Vision LabVIEW software and recorded for post-processing. The yeast cell was considered as a prolate spheroid, i.e., a solid of revolution generated by rotating an ellipse about its major axis. The dimensions measured were the major axis (distance between the poles) and the equatorial plane diameter, a and b, respectively. The dimensions did not vary significantly as function of IS and counter-ion used (calcium or sodium). The drag force may be computed with the Stokes equation, Eq. (1), based on the assumption of an infinite medium (free of walls). The drag force under those conditions is referred to as F_∞.

In a first stage of calculation, the particle may be considered as spherical, the prolate spheroid being described as an equivalent sphere with radius R_{eq}[33]

$$F_\infty = 6\pi\eta R_{eq} U, \tag{2}$$

$$R_{eq} = \frac{8(b/2)}{3}\left[-\frac{2\phi}{\phi-1} + \frac{2\phi^2-1}{(\phi^2-1)^{3/2}}\ln\left(\frac{\phi+\sqrt{\phi^2-1}}{\phi-\sqrt{\phi^2-1}}\right)\right]^{-1}, \tag{3}$$

with $\phi = a/b$. When $\phi = 1$ in the case of a sphere, $2R_{eq} = a = b$. Table I reports statistical values of a and b obtained from about 1000 measurements, providing values centered at 6.3 and 5.4 μm, respectively, and $R_{eq} = 5.6/2$.

Actually, in the flow, the longitudinal axis of the yeast cell takes an orientation parallel to the stream in order to reduce the cross-section area exposed to the flow. Accordingly, the drag force should be computed[33,34] by Eqs. (4) and (5)

TABLE I. Values (mean ± standard deviation (SD)) of yeast cell dimensions a and b of related parameters and of shape-drag correction factor K_s.

Parameter	Mean ± SD
a (μm)	6.35 ± 0.81
b (μm)	5.41 ± 0.64
$\phi = a/b$	1.17 ± 0.17
$(a+b)/2$ (μm)	5.88 ± 0.66
$2R_{eq}$ (μm)	5.59 ± 0.63
K_s	1.04 ± 0.03

$$F_{drag} = 3\pi\eta b U K_s, \tag{4}$$

$$K_s^{-1}(\tau_0) = -\frac{3}{4}\sqrt{\tau_0^2-1}\left[(\tau_0^2+1)\frac{1}{2}\ln\left[\frac{\tau_0+1}{\tau_0-1}\right] - \tau_0\right], \tag{5}$$

$$\tau_0(a,b) = \left[1-\left(\frac{a}{b}\right)^2\right]^{-1/2}. \tag{6}$$

In the case of a sphere, $\tau \to \infty$ and

$$K_s(\tau_0) \approx 1 + \frac{1}{10\tau_0^2} + \frac{109}{1400\tau_0^4} + \ldots \to 1, \tag{7}$$

according to the series computed by the MATHEMATICA® software (Wolfram Research Ltd., UK).

Table I presents statistical values of a/b ratios and of correction factors K_s with a mean value at 1.17 and 1.04, respectively. From Eqs. (1) to (4) and dimension data (Table I), $F_{drag}/F_\infty = bK_s/2R_{eq} = 1.002$. It appears thus that correcting for the shape of yeast is not needed.

Since the correction is negligible for dimension ratios that do not differ too much from unity, this methodology opens up new doors for the assessment of adhesion of yeast cells such as *S. cerevisiae, Candida albicans*, as well as bacteria like *Lactococcus lactis*[35] or spores of *Bacillus cereus*[36] for which the study of adhesion is a new emerging field.

3. Influence of the wall

When the force calibration is performed, a major parameter affecting the drag measurement is the distance of the cell to the wall, described by the Fáxen's law[33]

$$F_{drag} = F_\infty K_w, \tag{8}$$

$$K_w = [1 - (9/16)z_0 + (1/8)z_0^3 - (45/256)z_0^4 + (1/16)z_0^5]^{-1}, \quad z_0 = \left(\frac{b}{b+h}\right), \tag{9}$$

with K_w the wall correction and h the distance from the cell surface to the wall, here the substrate surface (see Fig. 1(b)).

Figure 2 presents the variation of the apparent drag force as a function of the distance to the wall, when the laser trap force was calibrated at a distance of 20 μm. The measurements were performed at different laser powers and the plotted data were either corrected (solid lines, closed symbols) using Eqs. (7) and (8) or not corrected (dashed lines, open

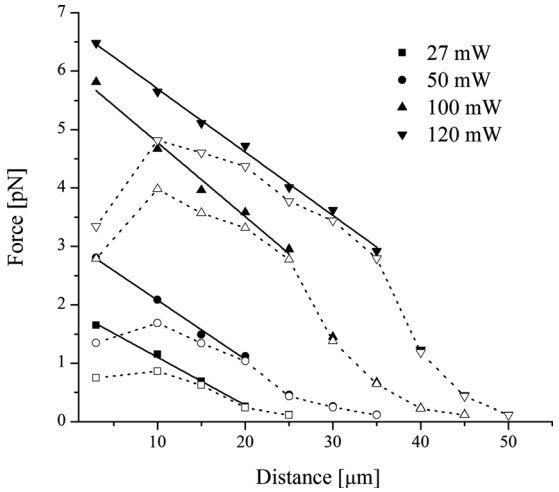

FIG. 2. Variation of the apparent drag force as a function of the distance to the wall, as deduced from measurements performed after calibrating the trap force at a distance of 20 μm from the wall, with (solid lines, closed symbols) or without (dashed lines, open symbols) correction for the hydrodynamic wall effect, at different laser powers in the sample.

symbols). It appears that even if a correction is made for the hydrodynamic effect of the wall, the relationship between the apparent trap force and the laser power varies with the distance to the wall. Note that at small distances (<20 to 40 μm), the slope shown by corrected values in Figure 2 is almost independent of the laser power, which means that the apparent escape force is linearly related to the laser power. At large distances, the apparent escape force drops dramatically although the correction for hydrodynamic effect is negligible.

Owing to these results, the validity of Eqs. (8) and (9) was examined by performing 3-D computational fluid dynamics (CFD), using Finite Element COMSOL Multiphysics 3.5 a package (COMSOL, Inc., Burlington, MA). Two models were considered: a sphere with the mean radius of R_{eq} and a prolate spheroid with the dimensions a and b reported in Table I. The steady laminar incompressible Navier-Stokes equations were solved using either Direct PARDISO or BigCStab solvers, depending on the memory allocated for the calculation. The boundary conditions were slipping conditions for the walls of the chamber (250 μm × 1 mm × 1 mm), inlet velocity set at $U = 92$ μm/s, outlet pressure set at atmospheric pressure and surfaces of the model particle considered as no-slip boundaries. Mesh consisted of 2–4 × 10^5 pyramidal elements. The drag force was post-processed by integrating the total axial force, i.e., the force along x axis, per area over y-z plane. The transversal force, i.e., the force along y axis, was found to be 0.01% to 0.1% of the drag force, which was supporting the quality of the meshed boundary of the particle. For tetrahedral elements, COMSOL Multiphysics computes the mesh quality as

$$q = 72\sqrt{3}V \Big/ \left(\sum_{1}^{6} h_i^2\right)^{3/2}, \qquad (10)$$

where V is the volume and h_1, h_2, h_3, h_4, h_5, and h_6 are the edge lengths of the tetrahedron. For a regular tetrahedron, q is equal to unity. The overall mesh quality indicator Q, given by the arithmetic mean by $Q = \sum_{i=1}^{N} q_i/N$, was not below 0.3.

The drag force was computed for spheroid and sphere models at different distances to the wall. Figure 3 provides a comparison between the drag correction factors F_{drag}/F_∞ given by the CFD and computed with Eqs. (8) and (9). It shows that deviation of cell shape from the sphere has no significant effect and that Eq. (9) accounts well for the hydrodynamic effect of the substrate surface. The hydrodynamic effect of the wall requires corrections by a factor that varies from 1.91 to 1.08 as the cell–substrate distance varies from 3 to 20 μm.

Figure 2 shows that despite appropriate correction for hydrodynamic wall effect, the apparent trap force decreases as the distance to the wall increases. This means that the trap stiffness declines with the distance. Therefore, correcting for the wall effect with Eqs. (8) and (9) is not sufficient in order to assess the force applied when the force calibration has been performed at another distance. This discrepancy may be attributed to spherical aberrations since the focal volume varies as a function of the distance to the wall.[37]

B. Practical determination of trap force

To improve trapping efficiency, oil-immersion objectives have a high numerical aperture (NA), most often around 1.35. However, such lenses give rise to spherical aberrations (SA), which are added to the total SA collected along the optical path. Since the indices of refraction of both the front lens of the objective and the immersion oil are the same, the main aberration comes from the interface between glass and the sample liquid.[37] The outermost rays, so-called marginal rays (Figure 1(c)), converge below the paraxial focus, resulting in a focal volume elongated by few micrometers along the z-axis. This focal volume gets more and more elongated

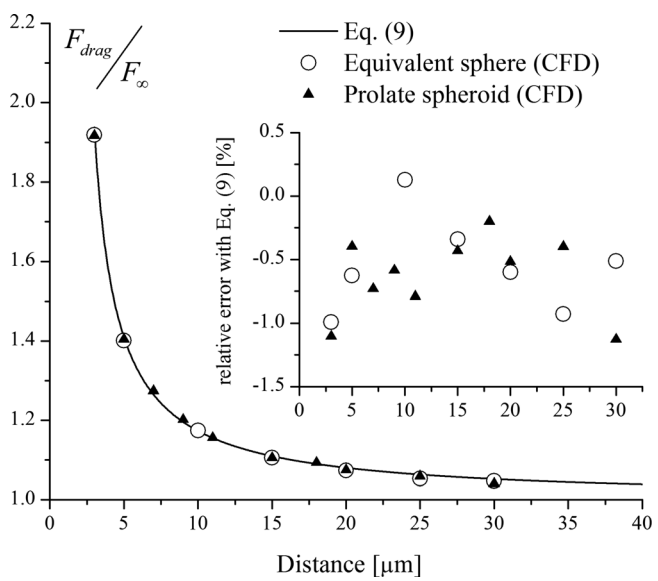

FIG. 3. Drag force correction for yeast cells as function of the distance to the wall, obtained by using Eq. (9) (solid line) and by CFD (sphere, open circles; prolate spheroid, solid triangles). Inset: relative difference between CFD results and results obtained using Eq. (9).

as the paraxial focus is set further from the surface. Such phenomenon affects strongly the trap efficiency, which decreases dramatically with the distance.

1. Adjusting the distance to the wall

For the usual force calibrations described below, the image plane was set at 20 μm from the surface, using the knob of the microscope. At this distance, the image of the yeast cell was blurry, due to spherical aberrations which bring the focus at a certain distance (focal shift) from the image plane. The focal shift was minimized by moving lens L_1 (Figure 1(a)) to get the sharpest yeast image, using a motorized linear stage (TGD00042/01/MV/TG/2 Newport, Irvine, CA). Thereby the cell could be placed at 20.0 ± 0.2 μm.

The effect of lens L_1 position deserves more explanation. Lens L_1 forms an afocal system with L_2. Translation of L_1 controls the divergence of the beam giving rise to the displacement of the beam focus along z-axis in the sample. Using the thin lens formalism, the focal plane translation, Δz, may be related to lens L_1 translation, Δd_{12}, by

$$\Delta z = \left(\frac{f_{obj}}{f_4}\right)^2 \frac{f_3}{f_2} \Delta d_{12}, \tag{11}$$

where f_2, f_3, f_4, and f_{obj} are the focal lengths of L_2, L_3, L_4, and L_{obj}, respectively. In our system, the distance d_{12} between lenses L_1 and L_2 was measured with a digital caliper (Mitutoyo SD-01, Kanagawa, Japan), providing $\Delta z/\Delta d_{12} = 6 \times 10^{-4}$.

2. Deducing the force exerted on adhering cells

For systematic experimental runs, it is convenient to calibrate the trap force at a certain distance from the substrate surface (chosen to be 20 μm) and to deduce the trap force at the distance relevant for adhering cells. The trap force at the distance of calibration (F^{calib}) and the trap force exerted on a non-adhering cell close to the substrate surface (F^{surf}) can be modeled by a linear function of the laser power P_{obj}[1]

$$\begin{aligned} F^{surf} &= a_1 P_{obj} + b_1, \\ F^{calib} &= a_2 P_{obj} + b_2. \end{aligned} \tag{12}$$

Figure 4(a) presents the plot of the trap force measured on cells located at 20 μm (closed squares) and on non-adhering cells located at 3 μm (closed circles), as deduced from Eq. (9), vs. the laser power. The linear regression parameters are $a_1 = 0.0535$ pN/mW, $b_1 = 2 \times 10^{-3}$ pN, $a_2 = 0.0462$ pN/mW, and $b_2 = -0.994$ pN.

The calibration graph obtained near the surface has a negligible intercept, i.e., the trap force near the surface is proportional to the laser power. The increase of the intercept as the distance to the surface increases is due to the increase of spherical aberrations, leading to an elongation of the focal volume. The random variation of experimental calibration data in Figure 4(a) with respect to the regression line is about constant in absolute value experimental data. The root mean square deviation is 0.16 and 0.22 pN at 20 μm and 3 μm, respectively. Note that the calibration graph at 3 μm was obtained from 4 sessions in which individual measurements

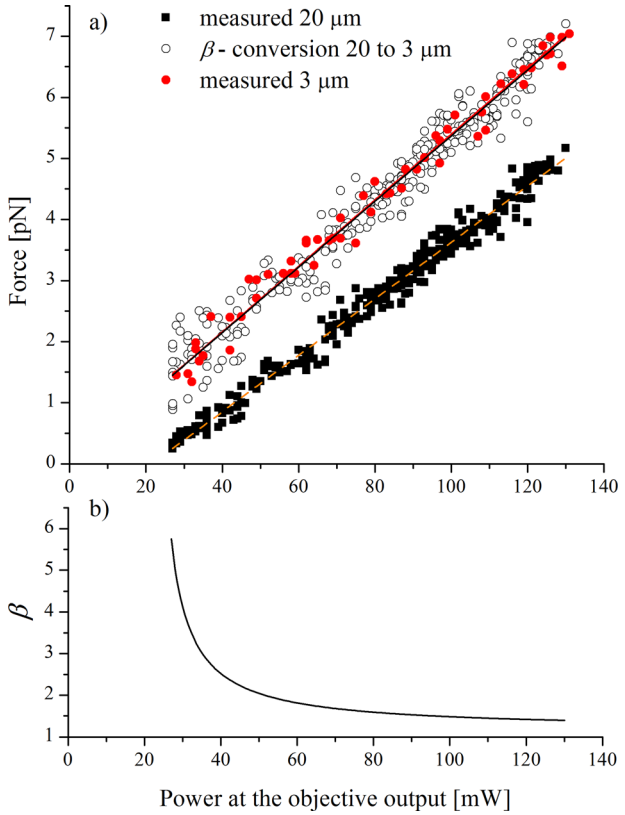

FIG. 4. (a) Wall-corrected drag force (pN) vs. laser power at the objective, measured at a distance of 3 μm (red closed circles) and 20 μm (black closed squares) from the surface. Experimental data taken at 20 μm and converted to the distance of 3 μm (open circles) though multiplication by β. (b) Conversion factor β described by Eq. (13).

were independent, while the calibration graph at 20 μm brings together data collected through the calibrations performed in numerous sessions of yeast adhesion experiments. Comparison of the two mean square deviations shows that the stability or setting of the instrument is not the main factor limiting the precision of the measurements. The latter seems to be limited by the operator appreciation of the particle escape from the trap.

For practical cell adhesion experiments, it is convenient to deduce the trap force near the surface F^{surf} from the trap force F^{calib} calibrated at a certain distance from the surface (chosen to be 20 μm)

$$\begin{aligned} F^{surf} &= \beta F^{calib}, \\ \beta &= 1 + \frac{(a_1 - a_2)P_{obj} + (b_1 - b_2)}{a_2 . P_{obj} + b_2}, \end{aligned} \tag{13}$$

where β is the force conversion factor from calibration to surface. Figure 4(b) shows the variation of β as a function of laser power. To illustrate the reliability of this conversion, the data taken at 20 μm (Figure 4(a), closed squares) were corrected with β (Figure 4(a), open circles) and compared with those taken at 3 μm (closed circles). The agreement between the measurements performed at 3 μm, and the data obtained at 20 μm and extended to 3 μm by correction with β are excellent (relative difference of slope equal to 0.46%), which supports the validity of the method and the reliability of β values. However, the broader dispersion of the data

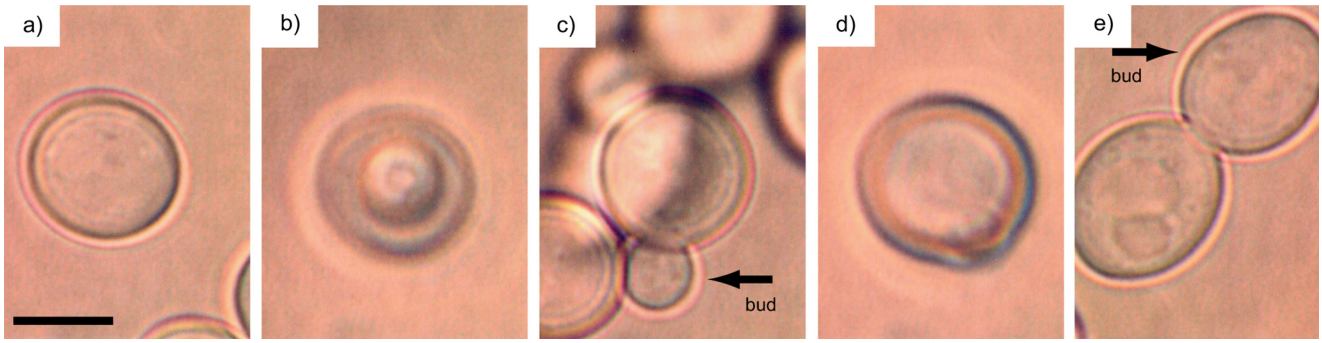

FIG. 5. Micrographs showing budding of a cell in the trap: time zero, $T_{in\ situ} = 30.1\,^{\circ}\mathrm{C}$ (a); after 3 h, $T_{in\ situ} = 30.3\,^{\circ}\mathrm{C}$, before (b) and after release and trapping again (c); after 5 h, $T_{in\ situ} = 30.2\,^{\circ}\mathrm{C}$, before (d) and after release and trapping again (e). Scale bar, 5 μm.

shows that the conversion of measurements at 20 μm to values at 3 μm leads to an increased random uncertainty on the value of the trap force, particularly at low laser power, owing to the strong increase of β at small distances.

For yeast adhesion measurements, we used the procedure consisting in calibrating the trap force with respect to laser power at a distance of 20 μm and converting it to a trap force at 3 μm. The laser powers used to define *non-adhering cells* (<27 mW) and *firmly adhering cells* (>120 mW), correspond to forces between 1.4 and 6.4 pN, respectively.

C. Evaluation of damage on the live cells

To investigate the possibly harmful effect of the optical trap on cells, a volume of cell suspension (from exponential phase culture) was inoculated in a fresh medium confined in a temperature-controlled chamber. The suspension was diluted to a starting concentration of 4×10^6 cells/ml. One cell was maintained trapped for up to 5 h. This experiment was performed 6 times. Figure 5 shows a typical result. In order to take adequate pictures, the cell was released after 3 h and trapped again; it was again released after 2 more hours and trapped again. Budding was observed, demonstrating that the 810-nm laser beam was not severely damaging the cell.

For a free cell in glucose minimal medium, the average doubling time of *S. cerevisiae* is 120 min at 30 °C.[38] The growth of yeast cells in the optical trap, after the bud initiation, is observed to be slower. We estimate that in the optical trap it will take approximately 5 h for a cell cycle. This difference could be due to the confinement and the subsequent lack of oxygen. Furthermore, as already mentioned by Singh *et al.*,[39] introducing yeast cells from exponential phase into a new medium might bring them into a lag phase, thus explaining the slower growth.

Recently, Singh *et al.*[39] and Volpe *et al.*[40] have studied the effect of the optical trap on the metabolic activity of *S. cerevisiae*. The power used was 5 mW for 3 h of trapping, whereas the maximum power used in the present study was 120 mW in the sample for 5 h. This confirms that the invasive effect of the optical trap is low since it is considered that the budding process reflects running metabolic activity.[39,40]

IV. APPLICATION TO YEAST CELL ADHESION

The aim of this section is to evaluate the possible advantage offered by examining the adhesion behavior of individual cells by OT, compared with common methods that are applied to a cell population as a whole. Therefore, the influence of ionic strength was examined in the light of DLVO (Derjaguin, Landau, Verwey, Overbeek) theory, which accounts for the influence of long distance interactions on the probability that approaching surfaces get attached together. An increase of ionic strength decreases the Debye length and is expected to decrease the electrostatic repulsion between negatively charged surfaces, leading to a repulsion barrier of reduced height with a maximum located at shorter distances.[41] In addition, the effect of calcium was compared to that of sodium. At the same ionic strength, divalent ions are indeed more efficient to reduce the effect or electrostatic repulsion (Schulze-Hardy rule). Moreover, calcium may act on the conformation of surface macromolecules, as shown by the role of specific (key-lock type) interactions in yeast flocculation.[42]

A. Surface properties

It has been demonstrated previously by scanning electron microscopy[19] that acid treatment does not alter the roughness of the glass surface. Therefore, this should not be modified by sulfochromic treatment.

The zeta-potential of the glass particles and of yeast cells is presented in Figure 6. The decrease of the absolute value of the zeta potential as a function of the ionic strength is in accordance with expectations.[43,44] The stronger effect of calcium, compared to sodium, may be attributed to an

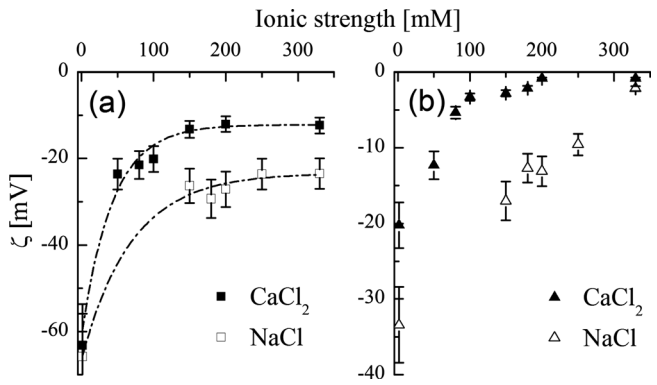

FIG. 6. Zeta potential (mV) as a function of ionic strength (mM) for (a) the glass particles and (b) the yeast cells, in the presence of NaCl (open symbols) or $CaCl_2$ (closed symbols). Dashed lines are decaying exponential fits.

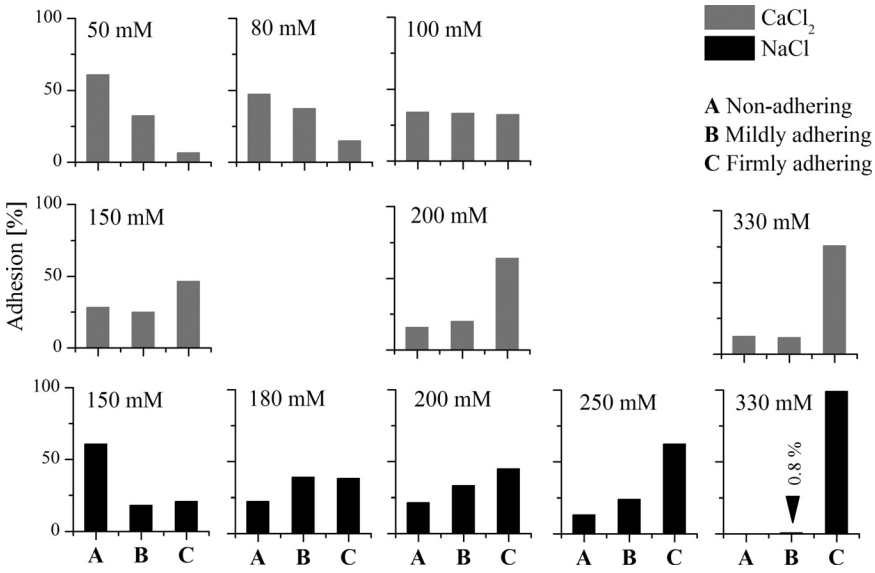

FIG. 7. Proportion of *firmly*, *mildly*, and *non-adhering* cells (%) ratioed to the total population, measured at 1 h contact time, at different $CaCl_2$ IS (50, 80, 100, 150, 200, and 330 mM) and NaCl IS (150, 180, 200, 250, and 330 mM).

enhanced adsorption in the Stern layer, which also explains the Schulze-Hardy rule.[41] The more pronounced effect of the salts on yeast compared to glass particles may be attributed to the fact that the yeast wall is subject to a penetration by water and ions, in contrast with glass.[45]

B. Proportion of adhering yeasts

The population analyzed has been defined as three groups: *non-adhering* cells, i.e., cells that are dragged away at the lowest laser power (27 mW), *firmly adhering* cells, i.e., cells that remain attached to the surface at the maximum laser power (120 mW), and *mildly adhering* cells, i.e., cells that are detached in the measurable range between 27 mW and 120 mW. Histograms representing the three mentioned groups are shown in Figure 7 as the proportion of cells ratioed to the total population analyzed after 1 h of contact at 25.5 ± 0.1 °C, for different ionic strengths imposed by NaCl and $CaCl_2$. The figure shows a clear shift of *non-adhering* to *firmly adhering* yeast cells as IS increases, the effect being appreciably stronger in $CaCl_2$ compared to NaCl. At 1.5 mM IS (NaCl and $CaCl_2$), adhesion was very weak and is not shown in the figure. In contrast, at 330 mM, 99% and 76% of cells were firmly attached in the presence of NaCl and $CaCl_2$, respectively.

C. Adherence of yeast

Figure 8 shows histograms presenting the distribution of *mildly adhering* cells as a function of removal force, after 1 h of contact time at different IS of $CaCl_2$ and NaCl. Here, the proportion of *mildly adhering* cells is normalized by the maximum value of each histogram (arbitrary units, a.u.). For each solution composition, detachment forces are spread

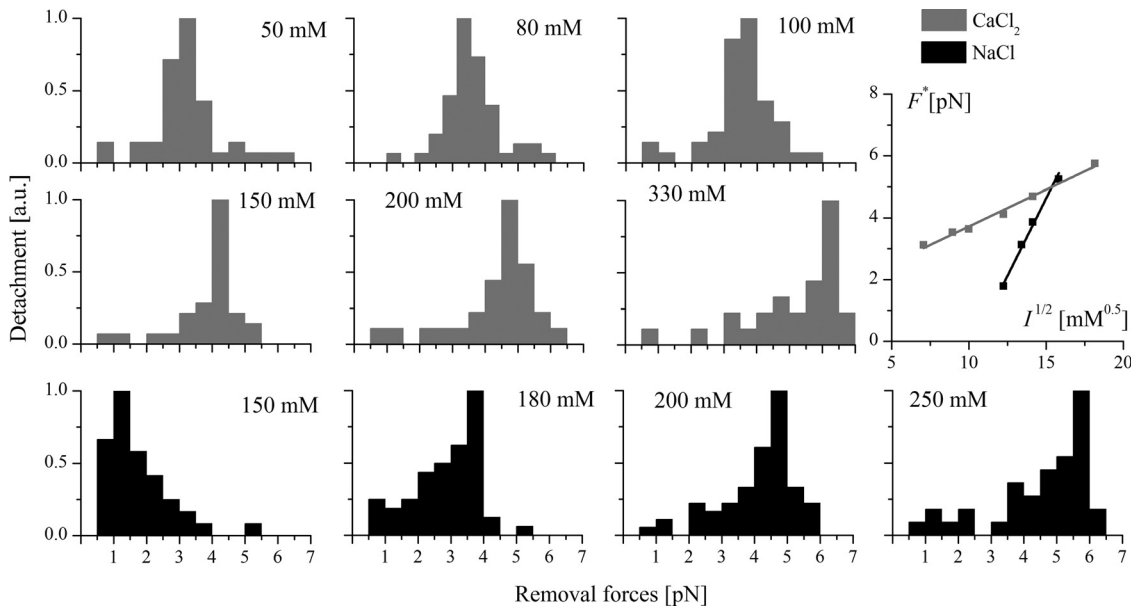

FIG. 8. Proportion of *mildly adhering* cells (in a.u., normalized by the maximum value) removed after 1 h contact time for different intervals of the applied force (pN) at different $CaCl_2$ IS (50, 80, 100, 150, 200, and 330 mM) and NaCl IS (150, 180, 200, and 250 mM). Inset: plots of the median detachment forces F^*(pN) vs. $\sqrt{IS}$(mM$^{0.5}$) with Ca and Na with linear fits (solid lines).

around a single maximum, which is shifted upwards when IS increases. The graph in inset shows that the median detachment force increases with the square root of IS, i.e., decreases as a function of Debye length. Moreover at a given ionic strength, the median detachment force is higher in $CaCl_2$ compared to NaCl. The difference is particularly marked at low ionic strength, which fits the idea of a strong interaction between calcium and surface sites.

V. DISCUSSION

A. Yeast cell adhesion

The proportion of adhering cells is related to the probability that cells pass the energy barrier created by electrostatic repulsion when a cell approaches the substrate by sedimentation or by Brownian motion. Its increase with the ionic strength (Figure 7) is in accordance with the expectations based on DLVO theory,[41] as illustrated by numerous examples.[26] The adhesion promotion of calcium was reported for several microorganisms involved in agroindustry, such as *Lactobacillus* spp. and *Escherichia coli*,[46] or in marine and groundwater environments, such as *Burkholderia cepacia* and *Halomonas pacifica*.[12] The enhanced effect of calcium compared to sodium is an illustration of the Schulze-Hardy rule. It may be attributed to chemical interactions or localized electrostatic interactions of calcium in the Stern layer. Alternately, if the surface is considered as penetrable to water and ions,[45] it may be due to formation of coordination bonds or ionic pairs. The three mechanisms are in agreement with a less negative zeta potential (Figure 6) and lead to a decrease of the electrostatic repulsion between the approaching yeast and the substrate.

The use of OT made it possible to measure not only the proportion of adhering cells but also the detachment force of individual cells. Both the removal of adhering cells (Figure 7, *firmly* vs. *mildly adhering* cells; Figure 8, removal force of *mildly adhering* cells) and the proportion of adhering cells (Figure 7) were found to be enhanced with an increase of ionic strength or in the presence of calcium compared to sodium. Many authors noticed that the presence of calcium increases the adhesiveness at interfaces with microorganisms. Kuznar and Elimenech[14] have shown that *Cryptosporidium parvum* oocysts adhered stronger to quartz in $CaCl_2$ solution than in NaCl solution. Gingell and Vince[47] have determined the separation distance between glass and *Dictyostelium* amoebae using infinite aperture interferometry and have demonstrated that separation distance decreased with IS and cation valency (Na^+, K^+, Ca^{2+}, Mg^{2+}, and La^{3+}).

This may tentatively be discussed further in the light of DLVO theory. Figure 9 presents the potential energy profile in NaCl 150 mM, computed by DLVO theory from experimental data (zeta-potential of both surfaces (Figure 6)) as described before[19] using the method proposed by van Oss[8] (where $\Delta G^{LW}_{\ell_0} = -3.7$ mJ/m^2 and $\gamma^{LW}_{liquid} = 21.8$ mJ/m^2 in this case). It also gives the force profile, computed as the derivative of the energy with respect to the separation distance. It shows the presence of a high potential energy barrier and of a secondary minimum at a distance of about 5 nm. Table II presents the characteristics of the curves—height of the barrier, maximum repulsion force associated to the barrier F_1, maximum attraction force associated to the secondary minimum F_2—computed at different ionic strengths of NaCl and $CaCl_2$.

In this conceptual frame, the *mildly adhering* and *firmly adhering* cells may tentatively be considered to be retained in the secondary minimum and in the primary well, respectively. This is in agreement with the trends observed at increasing NaCl ionic strengths. However, this is not the case with calcium; DLVO theory predicts a strong attractive system, without any barrier from 80 to 330 mM. At 80 mM, the system turns fully attractive, with negative potential energy following a monotonic function. This radical change is in contradiction with the observation of a progressive increase of the proportion of *firmly adhering* cells and of the removal force of *mildly adhering* cells. Additionally, F_2 is a few times larger than the removal forces measured.

Another possibility is that all adhering cells are retained in the primary potential well. The removal force should then be the force required to get the cells out of the well and to pass back the energy barrier. This is in contradiction with the

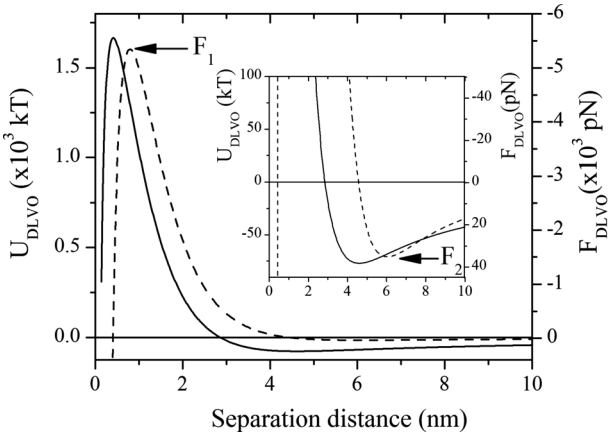

FIG. 9. Potential energy (left axis, 10^3 kT, solid line) and force (right axis, 10^3 pN, dashed line) computed by the DLVO theory as function of separation distance (nm) in NaCl 150 mM solution. Inset is a close-up of the figure.

TABLE II. Force level toward the barrier (nN), energy barrier (kT) and force level towards the secondary minimum (pN) as function of IS. *nb*, no barrier.

IS (mM)\force	Barrier F_1 (nN)	Energy barrier (kT)	Secondary minimum F_2 (pN)
Na^+			
1.5	−1.9	6802	0.1
150	−5.3	1665	35.1
180	−3.8	1055	45.2
200	−4.1	1080	51.2
250	−2	371	76.8
330	*nb*	*nb*	…
Ca^{2+}			
1.5	−1.4	2525	0.8
50	−1.3	222	66.4
80–330	*nb*	*nb*	…

fact that F_1 is 2 to 3 orders of magnitude higher than the measured removal forces and the latter is higher in $CaCl_2$, i.e., when there is no energy barrier.

As a matter of fact, comparison between measured removal force and computations is subject to much uncertainty. The removal force should be influenced by short distance interactions, the consideration of which is absent in DLVO theory and subject to criticism in extended DLVO theory.[26] One should also keep in mind that the surface of a microbial cell differs from that of a hydrophobic colloid and consists of biopolymers, which may be solvated to different extents.[45] Accordingly, the interactions of macromolecules at the interface play a crucial role. They may involve bonds between macromolecular segments and the substrate surface. Moreover, the cells may liberate macromolecules into the solution, which quickly condition the substrate surface by adsorption[26] and favor cell adhesion, as directly demonstrated for *Azospirillum brasilense*.[15] The attraction between the conditioned surface and the cells may in turn involve bridging between macromolecular segments,[26] which is favored by a higher ionic strength and by the presence of divalent cations. It may also involve specific interactions, as observed between mammalian cells and substrates conditioned by protein adsorption.[48]

Furthermore, the stress exerted to detach the cells is not perpendicular to the substrate surface. Thus, the removal forces do not refer to a neat rupture and DLVO simulation is of limited relevance. The stress application is a kind of shaking made by moving the laser beam back and forth parallel to the substrate surface. As a matter of fact, the cell detachment at low ionic strength involves slipping and rolling[19] offering similarities with a peeling process.[7,49] The presumable role of interactions involving macromolecules suggests that the removal forces should be influenced by relaxation processes at the interface. This could be investigated further as changing the amplitude of lateral motion and its frequency, which makes it possible to control separately the motion velocity (and thus the drag force) and the time scale of the perturbation imposed and thus to examine the influence of the loading rate.

The range of removal forces measured here (1 to 10 pN) may be put in perspective with respect to other forces that are relevant in bioadhesion processes. The rupture force of a single receptor-ligand pair is in the range of 20 to 200 pN; the force of unfolding a single protein molecule is in the range of 100 to 200 pN; the rupture force of a covalent bond is of the order of 4 nN.[50] Considering an apparent density of 1.07 g/cm^3 and a 5.6 μm diameter for yeast gives a force of gravity exerted on an individual cell equal to 63 fN. As a matter of fact, the pressure exerted by a yeast cell sediment was a possible explanation for the increase of the amount of yeast cells adhering to glass as a function of the thickness of the cell sediment produced before washing.[51] As microbial cells are subject to Brownian motion, a further interesting consideration may be made following the approach of sedimentation equilibrium.[41] The driving force for diffusion (inherent to Brownian motion) is given by $F_d = k_B T \mathrm{d}\ln C/\mathrm{d}z$, where z is a distance measured in the direction of the gradient of concentration C, k_B is the Boltzmann constant, and T the temperature. An arbitrary but meaningful way of evaluating F_d is to consider an increment of $\Delta \ln C = 1$ and an increment of $\Delta z =$ cell size, i.e., 5.6 μm. This is indeed the force that needs to be balanced for maintaining a significant cell concentration gradient. For a particle of yeast cell size, this is found to be 0.7 fN.

At this stage, one may address the fact that the occurrence of cell adhesion is not a matter of yes (100%) or no (0%) but is characterized by broad distribution functions (Figure 7). Note that the criterion used here to consider that a cell is adhering, i.e., a significant value of the removal force (1 pN), is much more reliable than the often used resistance to more or less controlled washing. Since early works,[52] the amount of adhering microorganisms has sometimes been presented in the form of adsorption isotherms (amount adhering vs. amount in the suspension) and fitted with the Langmuir equation, even if the hypotheses at the basis of Langmuir model (reversibility, 1 particle for 1 surface site, defined number of surface sites) are not fulfilled. Furthermore, the basic concept in the Langmuir model, which involves an equilibrium constant, supposes that a significant role is plaid by the entropy change associated with the dilution of particles in suspension and with the variation of the degree of occupation of surface sites. While this is the case for molecules and for small size colloidal particles, the practical influence of entropy and Brownian motion decreases as the particle size increases, as revealed by the decreasing relevance of sedimentation equilibrium. For yeast cells, it is negligible as illustrated by the comparison of the diffusion force ($\sim$1 fN) with the gravity force ($\sim$60 fN) and the removal force (1 to above 10 pN). The situation would be analogous for bacteria.

The time span of arrival of the cells close to the substrate may lead to a distribution of contact times, which could possibly explain the fact that some cells do and some do not adhere. In the present work, according to the rate of cell sedimentation (0.72 mm/min) and the distance between the slide and the coverslip (250 μm), cell settling must be completed in 3 min, which is much smaller than the delay of 1 h between assembling the sample and starting the measurements. Thus, mass transport may not explain the heterogeneity of cell behavior. Finally, according to the Random Sequential Adsorption (RSA) model,[53] the adhering amount might be controlled by the available substrate area, taking into account electrostatic repulsions between cells at the interface. In the present work, the average area available per cell settled on the surface is about 1000 μm^2, which means that the available area is about 30 times the area occupied per cell and that the average distance between cells is larger than 20 μm, i.e., in a range for which interactions between incoming cells and already settled cells are negligible. Thus, the RSA model does also not explain the heterogeneity of cell behavior. This must be attributed to a heterogeneity of surface properties at the cell level (genetic diversity, variation of gene expression, distribution of ages, random variation) or at the subcellular level. This may concern scars but also more subtle features, as shown by the presence of nanodomains of adhesin at the surface of *S. cerevisiae* and *C. albicans* and their role in cell aggregation and biofilm formation.[54] This interpretation is compatible with the fact that

the proportion of adhering cells and the removal force vary in the same direction according to the solution composition.

B. Force measurements with single cells

Magnetic tweezers (MT) and AFM emerged in the last decades in parallel to OT. AFM involves a cantilever terminated by a tip in contact with (or very close to) a surface; the deflection of the cantilever is recorded by a laser impinging a photodiode. MT involve the manipulation of magnetic particles by a magnetic field. An advanced version of MT is the electromagnetic tweezers, which permit free 3D translational (and rotational) manipulation and variation of magnetic field intensity. In OT and AFM, the force is exerted through a change of probe position. While the three techniques offer the important advantage of making measurements on individual cells, each of them offers specific performances. Table III summarizes the main characteristics of the three techniques; their advantages and limitations are discussed below.

The spatial resolution is dictated by the thermal fluctuations, which can be approximated as $\delta = \sqrt{k_B T/\kappa}$, where $k_B T$ is related to the Brownian motion and κ is the stiffness of the probe (OT and MT), and of the cantilever (AFM). Spatial resolution must be differentiated according to the orientation, axial (commonly the z-axis, normal to the surface), or lateral (along x and y axes). OT often exhibits an elongated focal volume, which results in stronger lateral trapping compared to axial trapping,[55] and a better lateral resolution (down to the DNA base-pair resolution[56]). Similarly, MT probes have a stronger lateral than axial stiffness.[57] AFM offers the possibility of imaging, which means that each single experiment along the axial direction (0.5 nm resolution) can be repeated over the surface according to pixel size or probe width (about 40 nm). In all three techniques, the position signal may be filtered from the power spectrum of the probe position oscillation, using the appropriate frequency bandwidth. The time resolution is inversely proportional to the bandwidth for the filtered signal.

AFM does not produce sample heating, in contrast with MT and OT. With the latter, the high intensity at the optical trap formed by the laser, typically 10^9–10^{12} W cm^{-1}, results in local heating. Likewise, MT produce a high magnetic field and require high-current electromagnets that may lead to substantial heating in the sample. The temperature rise can influence protein conformation and cell viability. It may also change the local viscosity of the medium and thus the force accuracy. Heating in the vicinity of the optical trap can be calculated,[58] and several techniques have been developed to measure the temperature directly.[58,59]

TABLE III. Comparison of single-cell techniques (modified from Ref. 68).

	OT	MT	AFM
Space resolution (nm)			
Axially	2	8	0.5
Laterally	0.5	2	40
Time resolution (s)	10^{-4}	10^{-4}–10^{-1}	10^{-3}
Use with cell as a probe			
Applicability	++	−	+
Stiffness (*pN nm*$^{-1}$)	10^{-3}–0.5		10^{-5}–10^{1}
Force range (*pN*)	0.1–100		10–10^4

OT, MT, and AFM have respective advantages depending on whether the cell is used as a probe, whether the cell surface is tested with a probe, or whether the aim is to probe inside the cell. Only the first situation, which is the case of this work, will be discussed here. Many approaches use the cell as a probe for the study of cell-cell or cell-substrate interactions. Optical tweezers offer the advantage of trapping a live cell, manipulating it in physiological conditions and measuring forces. The probe-cells may be any organism in the adequate range of size, namely, from 0.5 μm to 30 μm, for instance, bacteria and viruses,[60] yeast cells,[61] and red blood cells (RBC).[62] A single cell may also be transferred from a medium to another.[61] OT were used for malaria diagnosis by trapping self-rotating single RBC.[63] In contrast with the two other techniques, OT gives the possibility to study adhesion of a cell population by successive measurements on single cells in the same sample, which offers new perspective regarding the heterogeneity of behaviors, as illustrated in the present work, and provides relevant comparisons with flow chamber experiments or with natural and industrial systems.

Optical trapping of a cell may possibly induce photodamage, which is influenced by the time of exposure, the wavelength, the laser power, and the nature of the biological sample. For optical trapping of live cells, 830-nm and 970-nm wavelengths have been found to minimize photodamage in bacteria (*E. coli*)[64] and eukaryotic (Chinese hamster ovary) cells.[65] No evidence of photodamage or heating damage was found in the specific case of yeast cells[18] thanks to a trade-off among the operating parameters. In the present work, single yeast cells have been trapped in static culture medium during 5 h and budding was slowed down, possibly due to confinement itself. This result converges with the works of Singh *et al.*[39] and Volpe *et al.*[40] who demonstrated that trapping *S. cerevisiae* by laser tweezers only slowed down growth rate but did not affect the metabolic activity as monitored by Raman spectroscopy.

An important limitation affects the versatility and precision of OT owing to the purely optical origin of trapping. As the trap stiffness depends on the gradient of the optical field, perturbations that affect the intensity or the intensity distribution will degrade the performance of the optical tweezers. The influence of light scattering is illustrated by the fact that much higher trapping forces were obtained with dried and rehydrated cells compared to freshly cultured cells.[18] The optical heterogeneity of the cell (budding scars, organelles) will influence not only the range of forces available but also the trap stiffness. This property and its constancy over a cell population are thus crucial for the precision of OT measurements or for the interpretation of their distribution. Performances with cells are lower than those obtainable with homogenous beads and particles of high refractive index.[66]

As compared with OT, AFM presents severe limitations for using a cell as a probe, since the cell must be attached to the tip of the cantilever. This involves physical and/or chemical treatments, which are susceptible of altering the surface

and affecting cell viability. AFM has discriminated between specific and nonspecific rupture events between *L. lactis* bacteria and a substrate with adsorbed mucins.[35] However, measurements were not guaranteed to concern single cells. Likewise, the adherence of metabolically active *S. cerevisiae* cells to a native, a hydrophobic-coated, and a protein-coated mica substrate was quantified in an aqueous environment.[67]

In contrast with AFM, OT allows different cells to be used successively as probes in the same cell preparation. In essence, any dielectric particle near the focus of the trapping laser can be trapped. The drawback is that quickly diffusing particles have to be in low concentration to prevent additional objects from being trapped once the first object is captured. In the present work, the ease of picking up individual cells was one of the reasons for calibrating the trapping force at a distance (20 μm) above a layer of possibly settled cells.

A particularity of OT is to leave the trapped cell to rotate freely. Therefore, exerting a force parallel to the surface of the cell-probe partner (substrate or other cells) permits rolling during detachment, which simulates what occurs in shear-flow chambers.[21] On the other hand, the force may be exerted perpendicular to the partner surface if the laser beam is parallel to the latter.[19] OT thus allows different modes of detachment to be examined and compared regarding the removal force.

MT are not suitable to use a cell as probe, since magnetic particles are required. However, magnetic particles, possibly coated with macromolecules, may be used to simulate cells. In that context, MT offer certain possibilities detailed for OT.

VI. CONCLUSION

Trapping yeast cells with OT to study adhesion is not perturbed by cell wall deformation or cell deviation from a spherical shape. The trapping force may be calibrated by creating a harmonic oscillation and computing the drag force with Stokes law. The calibration of trap force vs. laser power is conveniently performed at a certain distance from the substrate; however, the hydrodynamic effect of the neighboring wall and spherical aberrations affecting the focal volume and the trap stiffness require correction to extend this calibration to adhering cells.

Yeast cells trapped for up to 5 h in our operating conditions were still able to undergo budding but showed an increase of doubling time. This may be due to confinement and depletion of oxygen rather than to photodamage and heating damage.

The application of optical tweezers to yeast cell adhesion showed the expected effect of the solution composition on the proportion of adhering cells. Its increase with the ionic strength and when sodium was substituted by calcium was expected from DLVO theory and Schulze-Hardy rule. It is also compatible with a penetration of water and ions into the subsurface. The detachment force increased in the same way. This observation and the fact that the detachment stress was exerted parallel to the substrate surface point to the role of interactions involving solvated macromolecules.

Both the proportion of adhering cells and the removal force showed a distribution which, in our experimental conditions, may neither be attributed to a distribution of cell-surface contact times due to mass transport kinetics nor be explained by the Random Sequential Adsorption model (RSA; limitation by the available substrate surface, taking account of electrostatic interactions between cells at the interface). It is attributed to heterogeneity of surface properties at the cell level or at the subcellular scale.

As compared with MT, AFM, and more conventional ways of studying cell adhesion (shear-flow cells), OT present several advantages: direct measurements in physiological conditions, clear criterion to evaluate the proportion of adhering cells, ease of examining the heterogeneity of cell behaviors in a population. However, the OT method is limited to low adherence forces (1 to 100 pN) owing to the low refractive index of cells and is sensitive to the cell optical heterogeneity. On the other hand, it opens exciting perspectives to investigate nanoscale and macromolecular aspects of cell detachment (influence of stress direction, relation between strain and stress, influence of time scale, and study of relaxation processes). MT is limited to models made by coating magnetic particles with biomolecules to simulate cell surfaces. AFM, which is well suited to investigate the heterogeneity of surface properties (electrical charges, hydrophobicity, macromolecules, and specific recognition sites) at the subcellular level, is less attractive than OT to directly study whole cell adhesion.

ACKNOWLEDGMENTS

The authors are grateful to Muriel Mercier-Bonin and Philippe Schmitz for providing the strains. The project was initiated in the Laboratoire de Rhéologie in Grenoble, and most of the measurements were performed there. Complementary data and numerical simulations were implemented in the Department of Physics in Umeå. Further data analysis was conducted in LISBP in Toulouse.

[1]A. Ashkin, Proc. Natl. Acad. Sci. U. S. A. **94**, 4853 (1997).
[2]C. Bustamante, J. C. Macosko, and G. J. L. Wuite, Nat. Rev. Mol. Cell Biol. **1**, 130 (2000).
[3]C. Gutsche, U. F. Keyser, K. Kegler, and F. Kremer, Phys. Rev. E **76** (2007).
[4]L. Sacconi, I. M. Tolic-Norrelykke, C. Stringari, R. Antolini, and F. S. Pavone, Appl. Opt. **44**, 2001 (2005).
[5]K. H. Simpson, G. Bowden, M. Höök, and B. Anvari, J. Bacteriol. **185**, 2031 (2003).
[6]A. Touhami, B. Hoffmann, A. Vasella, F. A. Denis, and Y. F. Dufrêne, Microbiology **149**, 2873 (2003).
[7]S. Lorthois, P. Schmitz, and E. Angles-Cano, J. Colloid Interface Sci. **241**, 52 (2001).
[8]C. J. van Oss, *Interfacial Forces in Aqueous Media*, 2nd ed. (Marcel Dekker, New York, NY, 1994).
[9]R. Bos, H. C. van der Mei, and H. J. Busscher, FEMS Microbiol. Rev. **23**, 179 (1999).
[10]S. Kang and H. Choi, Colloid Surf., B **46**, 70 (2005).
[11]M. Demilly, Y. Brechet, F. Bruckert, and L. Boulangé, Colloid Surf., B **51**, 71 (2006).
[12]G. Chen and S. L. Walker, Langmuir **23**, 7162 (2007).
[13]F. Ahimou, F. A. Denis, A. Touhami, and Y. F. Dufrêne, Langmuir **18**, 9937 (2002).
[14]Z. A. Kuznar and M. Elimelech, Environ. Sci. Technol. **38**, 6839 (2004).
[15]Y. F. Dufrêne, C. J. P. Boonaert, and P. G. Rouxhet, Colloid Surf., B **7**, 113 (1996).

[16]Y. F. Dufrêne, H. Vermeiren, J. Vanderleyden, and P. G. Rouxhet, Microbiology **142**, 855 (1996).
[17]A. M. Gallardo-Moreno, M. L. Gonzalez-Martin, C. Perez-Giraldo, E. Garduno, J. M. Bruque, and A. C. Gomez-Garcia, Appl. Environ. Microbiol. **68**, 2610 (2002).
[18]M. Castelain, F. Pignon, J. M. Piau, A. Magnin, M. Mercier-Bonin, and P. Schmitz, J. Chem. Phys. **127**, 135104 (2007).
[19]M. Castelain, F. Pignon, J. M. Piau, and A. Magnin, J. Chem. Phys. **128**, 135101 (2008).
[20]G. Guillemot, G. Vaca-Medina, H. Martin-Yken, A. Vernhet, P. Schmitz, and M. Mercier-Bonin, Colloid Surf., B **49**, 126 (2006).
[21]G. Guillemot, S. Lorthois, P. Schmitz, and M. Mercier-Bonin, Chem. Eng. Res. Des. **85**, 800 (2007).
[22]M. Mercier-Bonin, K. Ouazzani, P. Schmitz, and S. Lorthois, J. Colloid Interface Sci. **271**, 342 (2004).
[23]E. Fällman and O. Axner, Appl. Opt. **36**, 2107 (1997).
[24]T. B. Reynolds and G. R. Fink, Science **291**, 878 (2001).
[25]R. A. Speers, M. A. Tung, T. D. Durance, and G. G. Stewart, J. Inst. Brew. **98**, 293 (1992).
[26]C. J. P. Boonaert, Y. F. Dufrêne, and P. G. Rouxhet, *in Encyclopedia Environmental Microbiology—Biofilms*, edited by H. C. Flemming (Wiley, New York, 2002), p. 113.
[27]J. M. Piau, J. Non-Newtonian Fluid Mech. **144**, 1 (2007).
[28]E. Fällman, PhD thesis, Umeå University, 2001.
[29]E. Fällman, S. Schedin, J. Jass, M. Andersson, B. E. Uhlin, and O. Axner, Biosens. Bioelectron. **19**, 1429 (2004).
[30]M. Castelain, E. Koutris, M. Andersson, K. Wiklund, O. Bjornham, S. Schedin, and O. Axner, Chem. Phys. Chem. **10**, 1533 (2009).
[31]K. C. Neuman and S. M. Block, Rev. Sci. Instrum. **75**, 2787 (2004).
[32]A. E. Smith, Z. Zhang, C. R. Thomas, K. E. Moxham, and A. P. Middelberg, Proc. Natl. Acad. Sci. U. S. A. **97**, 9871 (2000).
[33]J. Happel and H. Brenner, *Low Reynolds Number Hydrodynamics: With Special Applications to Particulate Media* (Prenctice Hall, Englewood Cliffs, NJ, 1965).
[34]T. Aoi, J. Phys. Soc. Jpn. **10**, 119 (1955).
[35]E. Dague, D. T. Le, S. Zanna, P. Marcus, P. Loubière, and M. Mercier-Bonin, Langmuir **26**, 11010 (2010).
[36]C. Faille, C. Jullien, F. Fontaine, M. N. Bellon-Fontaine, C. Slomianny, and T. Benezech, Can. J. Microbiol. **48**, 728 (2002).
[37]E. Fällman and O. Axner, Appl. Opt. **42**, 3915 (2003).
[38]B. J. Brewer, E. Chlebowicz-Sledziewska, and W. L. Fangman, Mol. Microbiol. **4**, 2529 (1984).
[39]G. P. Singh, G. Volpe, C. M. Creely, H. Grotsch, I. M. Geli, and D. Petrov, J. Raman Spectrosc. **37**, 858 (2006).
[40]G. Volpe, G. P. Singh, and D. Petrov, Appl. Phys. Lett. **88**, 231106 (2006).
[41]P. Hiemenz and R. Ragagopalan, *Principles of Colloid and Surface Chemistry*, 3rd ed. (Marcel Dekker, 1997).
[42]K. J. Verstrepen and F. M. Klis, Mol. Microbiol. **60**, 5 (2006).
[43]J. Azeredo, J. Visser, and R. Oliveira, Colloid Surf., B **14**, 141 (1999).
[44]H. H. M. Rijnaarts, W. Norde, J. Lyklema, and A. J. B. Zehnder, Colloid Surf., B **14**, 179 (1999).
[45]J. F. L. Duval and F. Gaboriaud, Curr. Opin. Colloid Interface Sci. **15**, 184 (2010).
[46]N. Larsen, P. Nissen, and W. G. Willats, Int. J. Food Microbiol. **114**, 113 (2007).
[47]D. Gingell and S. Vince, J. Cell Sci. **54**, 299 (1982).
[48]J. L. Dewez, A. Doren, Y. J. Schneider, and P. G. Rouxhet, Biomaterials **20**, 547 (1999).
[49]E. Décavé, M. Demilly, B. Fourcade, F. Bruckert, L. Boulangé, and Y. Brechet, Philos. Mag. **85**, 3173 (2005).
[50]D. J. Muller, J. Helenius, D. Alsteens, and Y. F. Dufrêne, Nat. Chem. Biol. **5**, 383 (2009).
[51]P. G. Rouxhet, M. Mozes, M. P. Hermesse, and G. Matta-Amouri, in *4th European Congr. Biotechnology*, edited by O. M. Neijssel, R. R. v. d. Meer, and K. C. A. M. Luyben (Elsevier Science, Amsterdam, 1987),Vol. **2**, p. 193.
[52]*Microbial Adhesion to Surfaces*, edited by R. C. W. Berkeley, J. M. Lynch, J. Melling, P. R. Rutter, and B. Vincent (Ellis Horwood, 1980).
[53]C. A. Johnson and A. M. Lenhoff, J. Colloid Interface Sci. **179**, 587 (1996).
[54]M. C. Garcia, J. T. Lee, C. B. Ramsook, D. Alsteens, Y. F. Dufrêne, and P. N. Lipke, PLoS ONE **6**, e17632 (2011).
[55]S. N. S. Reihani and L. B. Oddershede, Opt. Lett. **32**, 1998 (2007).
[56]M. Mahamdeh and E. Schäffer, Opt. Express **17**, 17190 (2009).
[57]T. Strick, J. Allemand, V. Croquette, and D. Bensimon, Prog. Biophys. Mol. Biol. **74**, 115 (2000).
[58]E. J. Peterman, F. Gittes, and C. F. Schmidt, Biophys. J. **84**, 1308 (2003).
[59]Y. Seol, A. E. Carpenter, and T. T. Perkins, Opt. Lett. **31**, 2429 (2006).
[60]A. Ashkin and J. M. Dziedzic, Science **235**, 1517 (1987).
[61]E. Eriksson, K. Sott, F. Lundqvist, M. Sveningsson, J. Scrimgeour, D. Hanstorp, M. Goksor, and A. Graneli, Lab Chip **10**, 617 (2010).
[62]P. J. Bronkhorst, G. J. Streekstra, J. Grimbergen, E. J. Nijhof, J. J. Sixma, and G. J. Brakenhoff, Biophys. J. **69**, 1666 (1995).
[63]S. K. Mohanty, A. Uppal, and P. K. Gupta, Biotechnol. Lett. **26**, 971 (2004).
[64]K. C. Neuman, E. H. Chadd, G. F. Liou, K. Bergman, and S. M. Block, Biophys. J. **77**, 2856 (1999).
[65]H. Liang, K. T. Vu, P. Krishnan, T. C. Trang, D. Shin, S. Kimel, and M. W. Berns, Biophys. J. **70**, 1529 (1996).
[66]A. Jannasch, V. Bormuth, C. M. Van Kats, A. Van Blaaderen, J. Howard, and E. Shäffer, Proc. SPIE **7038**, 70382B (2008).
[67]W. R. Bowen, R. W. Lovitt, and C. J. Wright, J. Colloid Interface Sci. **237**, 54 (2001).
[68]K. C. Neuman and A. Nagy, Nat. Methods **5**, 491 (2008).